Comparison of SEM and HRTEM CD Measurements Extracted From Test Structures Having Feature Linewidths From 40 to 240 nm

Michael W. Cresswell, *Life Fellow, IEEE*, Richard A. Allen, *Senior Member, IEEE*, William F. Guthrie, Christine E. Murabito, Ronald G. Dixson, and Amy Hunt

***Abstract*—Critical dimension (CD) measurements have been extracted from SEM and high-resolution transmission electron microscopy (HRTEM) images of the same set of monocrystalline silicon features having linewidths between 40 and 240 nm. The silicon features are incorporated into a new test structure that has been designed to facilitate this type of CD metrology study. Major improvements to previously reported HRTEM sample-preparation and fringe-counting procedures have been implemented. The purpose of this paper is to make a preliminary assessment of the calibration statistics of SEM transfer metrology when HRTEM is used as the primary metrology in CD reference material calibration. The linearity and the correlation of the regression between HRTEM and SEM measurements were very encouraging. However, further study of the calibration statistics, from which uncertainty estimates of the SEM CD measurements were obtained, revealed small but significant test-chip-to-test-chip variability of the SEM-to-HRTEM offset at the low single-digit nanometer level. Further measurements made the case that this unanticipated variability originated in the differences in the amounts of hydrocarbon deposition that were made by the SEM tool during the measurement cycle. This is considered to be a very useful finding because modern SEM tools, which can reduce hydrocarbon deposition below levels that were encountered here by almost an order of magnitude, are now becoming available. The results reported here provide a strong indication that HRTEM–SEM-based calibration approaches offer great promise for single-digit nanometer uncertainty.**

Manuscript received February 28, 2006; revised August 6, 2007. For this paper, the authors have combined the material of two papers that they presented at the IEEE International Conference on Microelectronic Test Structures, Louvain, Belgium, in April 2005, with additional text and illustrations. This work was supported by the Office of Microelectronics Programs and the Advanced Technology Intramural Program, National Institute of Standards and Technology.

M. W. Cresswell is with the National Institute of Standards and Technology, Gaithersburg, MD 20899-8120 USA (e-mail: michael.cresswell@nist.gov).

R. A. Allen and C. E. Murabito are with the Semiconductor Electronics Division, Electronics and Electrical Engineering Laboratory, National Institute of Standards and Technology, Gaithersburg, MD 20899-8120 USA (e-mail: richard.allen@nist.gov).

W. F. Guthrie is with the Statistical Engineering Division, Information Technology Laboratory, National Institute of Standards and Technology, Gaithersburg, MD 20899-8980 USA (e-mail: will.guthrie@nist.gov).

R. G. Dixson is with the Precision Engineering Division, Manufacturing Engineering Laboratory, National Institute of Standards and Technology, Gaithersburg, MD 20899 USA.

A. Hunt is with the Accurel Systems International Corporation, Sunnyvale, CA 94085 USA.

Color versions of one or more of the figures in this paper are available online at http://ieeexplore.ieee.org.

Digital Object Identifier 10.1109/TIM.2007.908313

***Index Terms*—Atomic force microscopy (AFM), calibration, critical dimension (CD), dimensional standards, high-resolution transmission electron microscopy (HRTEM), lattice-plane selective etch, linewidth, metrology, reference materials, scanning electron microscopy (SEM), SCCDRM, single-crystal silicon, standard reference material, traceability.**

I. Background

THIS PAPER reports critical dimension (CD) measurements that have been made with two different types of CD metrology instruments on sets of images of monocrystalline silicon features having linewidths between 40 and 240 nm. The replication of the features in monocrystalline silicon provides them with unique geometrical properties that are highly desirable for the purpose of CD metrology studies at the nanometer level. They are incorporated into a new test structure that has been specifically designed for this application. The two different types of instruments that were used are SEM and high-resolution transmission electron microscope (HRTEM) imaging. The technical motivation for the broader project, of which this paper is one part, is calibrating CD reference materials with traceability to the SI meter. The technique of HRTEM imaging reveals the silicon lattice-plane counts of feature cross sections and, thus, the respective features' linewidths based on the known lattice-plane spacing [1], [2]. For this reason, HRTEM has become established as the primary metrology to provide direct reference to the SI meter. However, its application is destructive, and it, therefore, requires a transfer metrology.

Recently, atomic force microscopy (AFM) has proven to be the leading transfer metrology for this application [3]. Although it is nondestructive and is not as costly to apply as HRTEM imaging, its practice requires substantial investments in equipment and in highly specialized knowledge and skills for optimal performance. It is, therefore, not a low-cost option. Thus, alternative traceability paths to HRTEM measurements featuring a transfer metrology, such as SEM, are technically interesting and worthy of assessment for certain calibration applications having less-demanding uncertainty requirements. Regardless of which metrology path is used for traceability to the SI meter according to the methods established by the International Organization for Standardization, an important figure of merit is the uncertainty that is attributed to the CD value that has been calibrated. Ideally, all other things being equal, this value should be as small as possible.

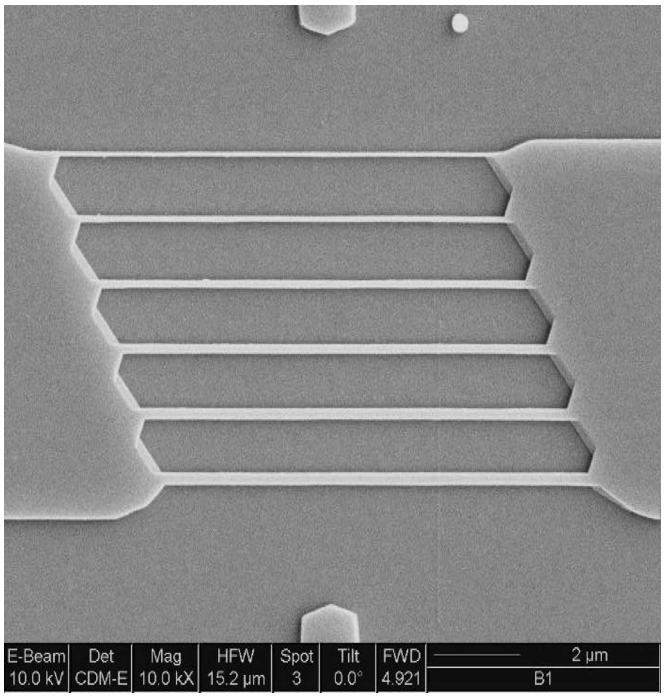

Fig. 1. SEM image of a test structure composed of six parallel features defined in the device layer of a (110) SIMOX wafer. The field areas are regions of the buried oxide that are revealed by patterning of the device layer.

II. Purpose

The specific purpose of this paper is to investigate the use of SEM imaging as an alternative transfer metrology. One application of this investigation would be the calibration of CD reference materials in special applications where, for example, the superior performance of AFM transfer metrology may not be needed, and/or there might be special motivation for cost control. In any case, an important figure of merit for a particular traceability path is characterized by the uncertainties that are attributed to the calibrated CD values. A specific purpose of this paper is to obtain an assessment of the CD uncertainties for the HRTEM/SEM traceability path and to compare this assessment with that provided by the recently established more accurate HRTEM/AFM alternative.

III. Test Chip Design and Fabrication

A. Test Chip Design

The new test structure used in this project was designed to facilitate CD extraction from six features, having drawn linewidths staggered by 30 nm, from a single HRTEM image. This arrangement is beneficial because HRTEM imaging to reveal silicon lattice-plane counts, besides being destructive, is very much resource consuming. Factors driving the geometry of the design of the test structure, a perspective image of which is illustrated in Fig. 1, result from the orientation of its principal axes to $\langle 112 \rangle$ lattice vectors in the (110) surface of the separation by implantation with an oxygen (SIMOX) wafer [4].

This arrangement is responsible for the diamond-like appearance of various features of the test chip, whose design is designated as NIST45, as shown in Fig. 2. This figure shows one half of the test chip. The other half is a left-to-right mirror image of the same layout.

B. Fabrication Process

The test chip pattern is replicated in the device layer of a 150-mm diameter (110) SIMOX wafer. The nominal height of all the reference features is 150 nm. The device layer is electrically isolated from the remaining thickness of the substrate by a 390-nm-thick buried oxide created by oxygen implantation.

Fabrication begins with the growth of a nominally 20-nm-thick oxide film to serve as a hard-mask material. The test chip image, of which one half is shown in Fig. 2, is then projected into resist so that its principal axes are oriented to a $\langle 112 \rangle$ lattice direction.

The latter is established by transfer of an orientation fiducial pattern firstly to the hard mask and then to the silicon with a deep lattice-plane selective etch. This operation is followed by visual inspection of the pattern's features. After the resist image of the test chip is transferred to the hard mask, the latter's features are replicated in the p-type silicon surface layer of the substrate by lattice-plane selective etching. Tetramethylammonium hydroxide etches (111) silicon lattice planes at a rate 10–50 times more slowly than it etches other planes such as the (110) surface of the wafer, allowing the (111) planes of the reference-feature sidewalls to behave as lateral etch stops. Aligning reference features with $\langle 112 \rangle$ lattice vectors in the (110) surface of the wafer results in their having planar vertical (111) sidewalls. Additional details of the substrate orientation specifications and the patterning process have been described elsewhere [4].

IV. CD Measurement Procedures

A. CD Extraction by SEM Image Analysis

Fig. 3 shows a pair of adjoined top-down SEM images of a single test structure rotated by 90° relative to the one shown in Fig. 1. Lateral locations along 0.5-μm-long central sections of each of the six features are referenced by the two markers. For the purpose of extracting SEM CD measurements, the images of these central sections are first converted into a binary form with commercially available image-processing software. Proprietary code is then used to extract local linewidths from these binary images at points along the central section; these points have a 25-nm pitch, thus providing 40 CD measurements per micrometer.

B. Extracting Absolute CD Measurements From HRTEM Images

1) Sample Preparation and HRTEM Imaging: The HRTEM measurement procedure begins after the completion of the measurements that make up the transfer metrology (in this case SEM) because HRTEM is a destructive procedure [5].

The test chip is prepared for HRTEM using a process that has been optimized to ensure that the surfaces of the reference feature are not damaged. Each step of this three-step process serves to define the region and protect the sidewalls of the

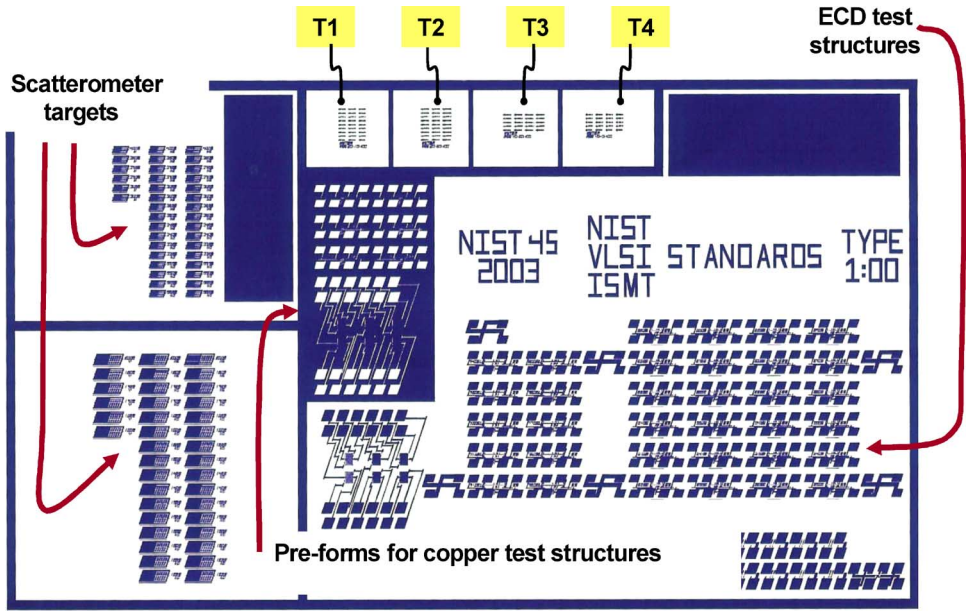

Fig. 2. Upper (1:00) section of the NIST45 SCCDRM chip layout has, among other structures, the HRTEM target arrays T1.

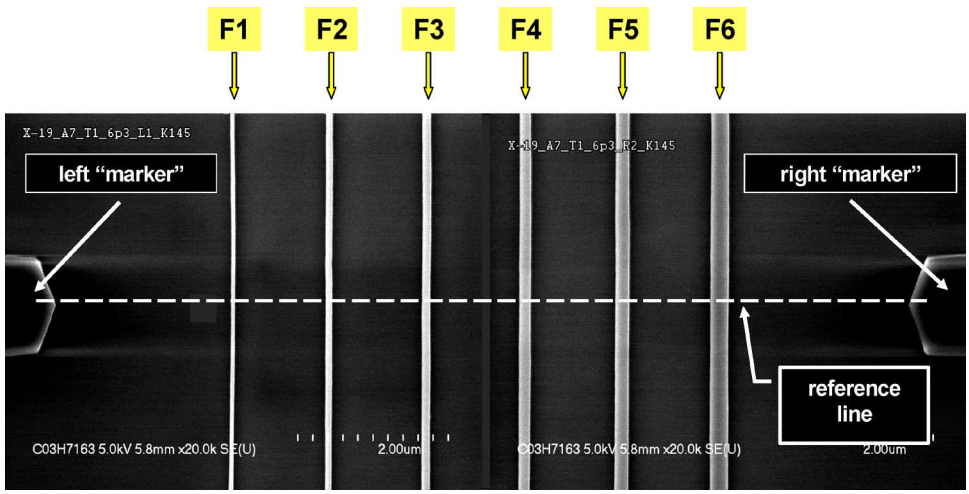

Fig. 3. Locations of central sections of each of the six features F1 through F6, which are usually 1 μm long, are referenced by the two markers.

features from the subsequent higher energy thinning steps. The first step is deposition, by sputtering or evaporation, of a gold–palladium film to protect the surfaces of the reference feature during the process steps that follow. After coating, the sample is placed in a focused ion beam (FIB)/SEM tool to mark the exact location for cross-sectioning with a rectangle that is approximately 0.5 $\times$ 8 μm in size, consisting of an electron-beam-assisted platinum film. This film is centered as closely as possible on the reference line that has been shown in Fig. 3. The final deposition step is that of a large 8 $\times$ 20 μm protective platinum rectangle that extends over the central region of the test structure.

At this point, the test chip is removed from the FIB/SEM and tripod polished to a thickness of 30 μm, both in the direction of the cross section and from the backside of the wafer. This 30-μm-thick sliver is then silver mounted on a half-grid and returned to the FIB/SEM and thinned as shown in Fig. 4(a) and (b). Fig. 4(c) shows the final orientation of the thinned regions with respect to the electron beam that is used for imaging in the HRTEM.

The sliver is then thinned along the axis perpendicular to the desired cross section. At the beginning of this process, a 30-kV gallium beam is used for rapid thinning; a 10-kV beam is used for the final thinning to prevent damage to the reference features. This thinning targets the center of the 0.5-μm region that is defined by the electron-assisted platinum mark and continues until the reference features become electron transparent.

Seven images were made of each HRTEM test structure: The first was a low-magnification (10 000$\times$) image showing all six of the reference features. An example of one of these, which shows the six-feature array in cross section, is given in Fig. 5. Each of the six reference features is clearly visible. Subsequently, six high-magnification images (one of each of the individual reference features in each test structure) were captured between 400 000$\times$ and 600 000$\times$. These were imaged on 80 $\times$ 100 mm negatives that were scanned at 900 dpi.

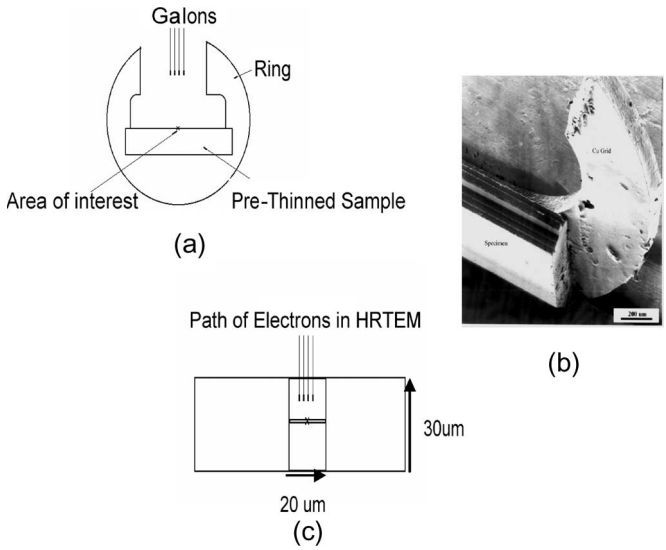

Fig. 4. This 30-μm-thick sliver is silver mounted on a half-grid and returned to the FIB/SEM and thinned, as shown in (a) and (b). The final orientation of the thinned regions with respect to the electron beam used for imaging in the HRTEM is shown in (c).

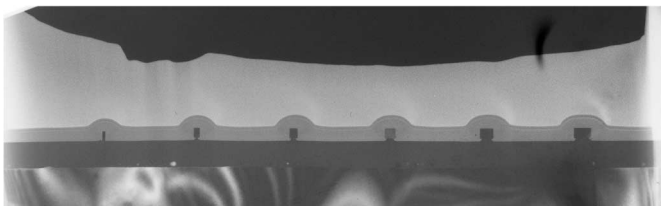

Fig. 5. Low-magnification HRTEM image of the complete cross section of a test structure.

This procedure enabled imaging each of the features with enough detail to enable the resolution of the silicon lattice. The high-magnification (400 000×) image of the narrowest of these reference features is shown in Fig. 6. A portion of the edge region showing the silicon lattice and the transition to the surrounding native oxide and deposited platinum is shown in the inset in Fig. 6.

2) CD Extraction From HRTEM Images: In previous work, we reported the progress in developing an image-processing procedure for determining the HRTEM fringe counts [6]. However, it was decided for this paper that an improved manual counting procedure would minimize the combined uncertainty. In contrast to the *ad hoc* counting procedure that was previously used, where the lattice count at the middle for each feature was measured by one of several operators, four operators would count the lattice planes in each reference feature at the top, middle, and bottom of the feature [5]. Four operators were used to ensure a reasonable minimum number of degrees of freedom in case the uncertainties in the HRTEM measurements were not consistent. If this had been the case, the individual measurements could not have been pooled into a single uncertainty measurement. Furthermore, beyond the lattice count, each operator would calculate the total feature width, including the native oxide, at the top, middle, and bottom of each feature. This improved procedure contrasts with the earlier one in which electrical CD (ECD) served as the transfer metrology, and

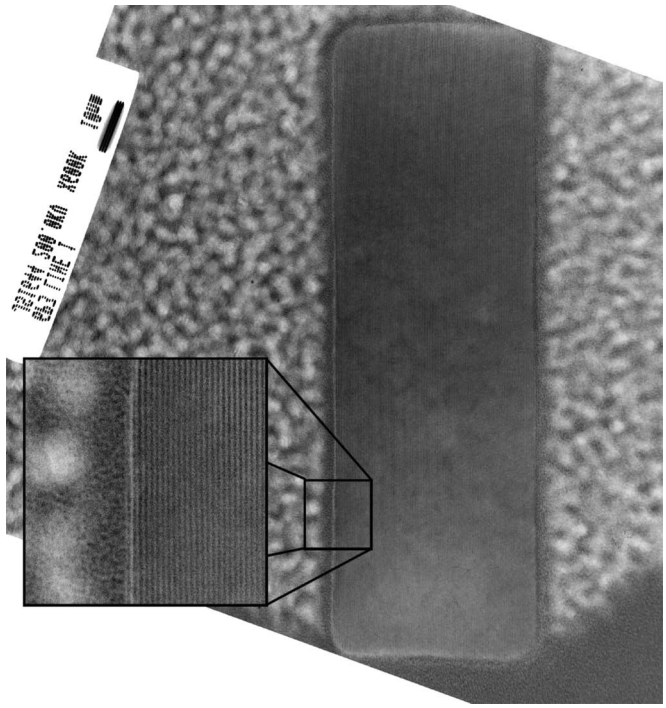

Fig. 6. High-magnification (400 000×) image of the narrowest of the reference features that are shown in Fig. 5.

HRTEM CDs were determined at a single location on the cross section from the visible fringe count. ECD is only a measure of the conducting path width in contrast to the total physical CD, as recorded by AFM or SEM, which includes the native oxide on the sidewalls of the feature. A total of 24 reference features of four HRTEM targets, each on a different chip and ranging in CD from 46 to 246 nm, were measured in this way.

Each operator began a lattice count with an image file that could be annotated to show features of interest and lattice-plane counts with a photoediting program. The cross section of each feature, including oxide, can be divided into three regions: the lattice region, the oxide region, and the transition region, each of which must be separately considered in the width determination. The lattice region is the major portion of the feature and consists of the region where the lattice is generally visible. The oxide region is the region of the feature that is primarily oxide, but contains partial lattice planes at the transition between oxide and silicon. The transition region is the transition between the oxide and the sputtered gold–palladium film. The lattice count procedure proceeded as follows: A surround box, which is the minimum-size box that can be drawn, which encompasses the entire structure including the oxide as well as a portion of the gold–palladium film, was drawn on each enlarged HRTEM image. The surround box, as well as other dimensions used in the count as described in the following paragraphs, is shown in Fig. 7. The size of each of the surround boxes was agreed upon by all operators. The remaining steps, however, were all independently performed by each operator.

In the second step, each operator identified the two outmost complete lattice planes. These lattice planes (one near each sidewall of the feature) are the ones closest to the sidewalls that can be visually followed from the top of the reference feature

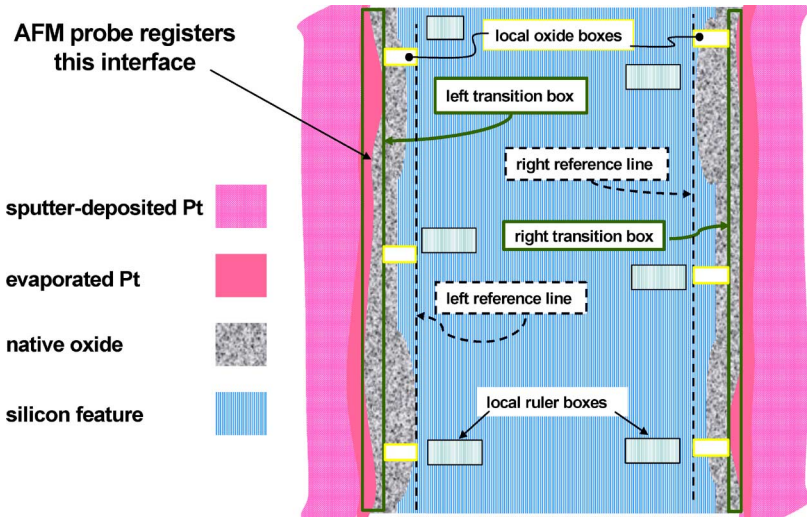

Fig. 7. Surround box, which is the minimum size box that can be drawn, which encompasses the entire structure including the oxide as well as a portion of the gold–palladium film, was drawn on each structure. It extends to outer edges of the two transition boxes.

to the bottom. A count of the lattice fringes was made between these two planes as near to the top and as near to the bottom of the feature as was feasible. The operators were asked to verify their counts if they differed by more than two lattice planes.

In the third step, each operator defined two transition boxes, one on each sidewall. The transition boxes encompass the region where there is an oxide-to-gold–palladium film transition. In other words, the outer limit of the oxide must be contained within the transition box.

In the fourth step, local oxide boxes are drawn from the reference lines to the inner edges of the respective transition boxes.

In the final measurement step, the oxide and transition regions are measured at the top, middle, and bottom of both sides of the feature. At each of these six locations, the operator determined the dimension (in units of "silicon lattice planes") by comparing the number of pixels in each of these boxes with the number of pixels in a number of lattice planes, as locally measured. Practically, this was done by drawing a "ruler box" around a given number of lattice planes and determining the size of this box (in units of pixels). It is of critical importance to locally determine this number, as the count can vary across the negative due to distortion in the imaging process.

At this point, all the raw data, that is, the various dimensions (in units of lattice counts), were input into a spreadsheet, and the CDs (in nanometers) were determined for the top, middle, and bottom of each feature. The transformation of the raw data to nanometers was accomplished with the formula

$$\mathrm{CD}_{\mathrm{HRTEM}} = \left(w_{\mathrm{RS}} + \sum_{j=1}^{2} \frac{1}{3} \sum_{i=1}^{3} \left(\frac{w_{\mathrm{TB}}^{j}}{2} + w_{\mathrm{OB}}^{i,j} \right) * R_{\mathrm{FPX}}^{i,j} \right) * R_{\mathrm{nmF}}$$

where

w_{TB}^{j} widths of transition boxes (in pixels);
w_{RS} separation of reference lines (lattice planes);
$w_{\mathrm{OB}}^{i,j}$ average width of oxide boxes (in pixels);
$R_{\mathrm{FPX}}^{i,j}$ local pixel-to-fringe conversion factor.

The calculations of the CDs in the spreadsheet were verified by an independent calculation of the CDs for one of the operators. The results for the first counting cycle are shown in Table I. Note that in Table I, there are six entries of "no data," which resulted from Counter 3 having been away from work for a time. The decision to continue with the remaining three counters in lieu of replacing this counter and asking the replacement to count the features on at least one chip that was already completed was made. This reduction was acceptable since the data up to this point indicated that the uncertainty was constant across CDs, allowing the pooling of data and making the need for four counters less critical.

The counters agreed on the results for 17 of the 24 features, where agreement was defined as less than 1 nm standard deviation. However, for the seven features where the standard deviation was higher (indicated in Table I by single boxes), the counters were asked to repeat their measurements. Although for most of these features it was a single counter who provided the outlier, all counters were asked to verify their counts. At this point, the counters were not told anything about how their original data compared with those of the other counters.

After the recounts, the average CDs were calculated, and the final results were compiled. In several of the original counts, there was a single outlier, which was lower than the counts provided by the other counters, although the other counters' results were generally in good agreement. In each of these cases, the counters had marked groups of lattice planes on their copy of the images; for example, groups of 20 lattice planes might have been marked. When these groups were counted, one or more were accidentally excluded. Upon including these missed counts, the results fell in line with those of the other counters.

The postrecount results for the individual counters as well as the averages and standard deviations for all counters are shown in Table II. For all of the features, postrecount standard deviations are less than the target of 1 nm. The exception is K145 C7 T1 6p3-f6, which is reported as "no data"; all three counters reported this feature to be among the most difficult of

TABLE I
RESULTS OF HRTEM CD MEASUREMENTS AFTER THE FIRST COUNTING CYCLE

Chip	Feature	Average (nm)	Standard Deviation	Individual Width (nm)				Maximum Difference
				Counter 1	Counter 2	Counter 3	Counter 4	
K145 A7 T1 6p3	F1	45.7	0.3	45.8	45.9	45.3	45.6	0.6
	F2	84.0	0.9	84.0	83.9	83.0	85.2	2.2
	F3	109.5	0.5	110.1	109.3	109.3	109.1	1.0
	F4	147.1	0.6	147.7	147.2	147.1	146.3	1.4
	F5	184.0	0.6	184.8	183.5	183.8	183.9	1.3
	F6	231.4	17.2	240.7	205.7	239.7	239.7	35.0
K145 C7 T1 6p3	F1	56.4	0.3	56.7	56.4	NO	56.2	0.5
	F2	98.2	0.4	98.4	98.4	NO	97.8	0.7
	F3	122.5	0.5	123.1	122.4	NO	122.1	1.0
	F4	171.0	3.6	173.1	173.0	NO	166.9	6.2
	F5	197.7	0.3	197.8	197.3	NO	197.8	0.6
	F6	245.3	5.4	249.0	247.9	NO	239.1	9.9

the 24 to count the lattice planes, and after recounts, the results still were in significant disagreement.

V. CALIBRATED CD MEASUREMENTS AND UNCERTAINTY ANALYSIS

The material in this section describes the methods for obtaining calibrated CDs from SEM transfer metrology point estimates and how the associated uncertainties are extracted from the results of a regression model, which is referred to as the calibration curve. In this exercise, the dependent and independent variables were SEM and HRTEM CD measurements. They were extracted from four six-feature test structures on four different chips, which, thus, provided a total of 24 data points, as described above. The impact of hydrocarbon contamination that is characteristic of SEM measurements is also described here.

A. Estimating CD Uncertainty From the Calibration Curve

The calibration curve is represented as a linear model given by the relationship

$$y = \beta_0 + \beta_1(x + \delta) + \varepsilon \tag{1}$$

where

- y CD determined from the SEM image;
- x CD determined from the HRTEM image;
- β_0 intercept of regression line;
- β_1 slope of regression line;
- δ random measurement error in x that is independent of ε and distributed with a mean of zero and variance σ_δ^2;
- ε random measurement error in y that is independent of δ and distributed with a mean of zero and variance σ_ε^2.

Equation (2) becomes a means of predicting an equivalent HRTEM-calibrated measurement x_0 from a "new" SEM transfer metrology measurement y_0. The point estimate of the calibrated measurement is obtained by solving

$$y_0 = \hat{\beta}_0 + \hat{\beta}_1 x_0 \tag{2}$$

for x_0 after fitting the model using Mandel regression [7]–[10], which accounts for the random errors in the dependent and independent variables in the fit. The quantities $\hat{\beta}_0$ and $\hat{\beta}_1$ are the estimates of the intercept and slope, respectively, which are obtained from the results of the Mandel regression.

The expanded uncertainty that is attributed to the point estimate x_0 is given by [8], [9]

$$U(x_0) = z_\alpha \sqrt{\frac{s_e^2}{\hat{\beta}_1^2} + \frac{D^2}{\hat{\beta}_1^2}\left(\frac{1}{n} + \frac{P^2(y_0 - \overline{y})^2}{\hat{\beta}_1^2 Q}\right)} \tag{3}$$

where

- z_α coverage factor from the normal distribution with a significance level of α;
- s_e $= (D\sqrt{\sigma_\varepsilon^2/\sigma_\delta^2})/\sqrt{P}$;
- D $= \sum_{i=1}^{n}(y_i - \hat{\beta}_0 - \hat{\beta}_1 x_i)^2/(n-2)$;
- n number of observations in the calibration data set;

TABLE II
POSTRECOUNT RESULTS FOR THE INDIVIDUAL COUNTERS AS WELL AS THE AVERAGES AND STANDARD DEVIATIONS FOR ALL COUNTERS

Chip	Feature	Average (nm)	Standard Deviation (nm)	Individual Width (nm)				Maximum difference (nm)
				Counter 1	Counter 2	Counter 3	Counter 4	
K145 A7 T1 6p3	f1	45.7	0.3	45.8	45.9	45.3	45.6	0.6
	f2	84	0.9	84	83.9	83	85.2	2.2
	f3	109.5	0.5	110.1	109.3	109.3	109.1	1
	f4	147.1	0.6	147.7	147.2	147.1	146.3	1.4
	f5	184	0.6	184.8	183.5	183.8	183.9	1.3
	f6	239.8	0.7	240.7	239.1	239.7	239.7	1.6
K145 C7 T1 6p3	f1	56.4	0.3	56.7	56.4	NO DATA	56.2	0.5
	f2	98.2	0.4	98.4	98.4	NO DATA	97.8	0.7
	f3	122.5	0.5	123.1	122.4	NO DATA	122.1	1
	f4	173.1	0.1	173.1	173	NO DATA	173.2	0.1
	f5	197.7	0.3	197.8	197.3	NO DATA	197.8	0.6
	f6	NO	NO	NO	NO	NO	NO	NO DATA

P $= (\sigma_\varepsilon^2/\sigma_\delta^2) + \hat{\beta}_1^2$;
$\overline{y}$ sample mean of the y_i values in the calibration data set;
Q $= (\sigma_\varepsilon^2/\sigma_\delta^2)^2 \sum_{i=1}^{n}(x_i - \overline{x})^2 + 2(\sigma_\varepsilon^2/\sigma_\delta^2)\hat{\beta}_1 \sum_{i=1}^{n}(x_i - \overline{x})(y_i - \overline{y}) + \hat{\beta}_1^2 \sum_{i=1}^{n}(y_i - \overline{y})^2$.

Since different tables and software for the normal distribution are parameterized in different ways, a numerical illustration is useful to guide the selection of the correct coverage factor. For example, when the desired confidence level is 95% (i.e., $\alpha = 1 - 0.95 = 0.05$), the appropriate two-tailed normal distribution coverage factor is $z_{0.05} = 1.96$.

B. Calibration Example

A trial implementation of the procedure described in Section V-A was fitting a straight-line calibration model to $n = 24$ pairs of measured HRTEM CDs and SEM CDs that were generated during the course of the broader project to use HRTEM with AFM to establish the CD traceability of these reference features. A plot of the data and the fitted regression line is shown in Fig. 8.

Without any further consideration of the statistics from the fit of the regression model, which is illustrated in Fig. 8, the expanded uncertainties that would be attributed to the results predicted by (2) through the use of (3) would have been approximately 11, 13, and 16 nm for confidence levels of 90%, 95%, and 98%, respectively. However, the following section reports why an analysis of the residuals of the fit in this case, at least partially, invalidates drawing such inferences from the available data.

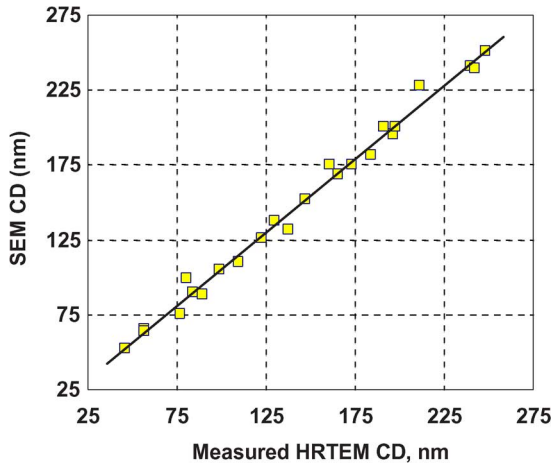

Fig. 8. Mandel regression line of SEM CD versus HRTEM CD.

Although the plot of the data with the regression function offers some ability to assess the fit of the model to the data, it is critical to also look at the plots of the residual errors from the fit r_i defined by the formula

$$r_i = y_i - \hat{\beta}_0 - \hat{\beta}_1 \left(x_i + \frac{\hat{\beta}_1}{P}(y_i - \hat{\beta}_0 - \hat{\beta}_1 x_i) \right) \qquad (4)$$

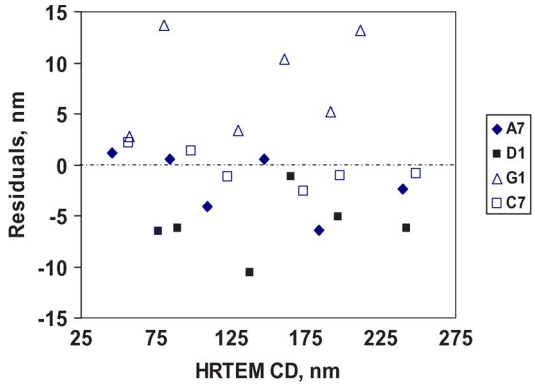

Fig. 9. Residuals from the model illustrated in Fig. 8 plotted versus the estimated HRTEM CD values illustrate the characteristics of the linear fit of SEM CD to HRTEM CD.

where y_i and x_i are the measured SEM and HRTEM CDs, respectively. If the model fits the data, the residuals should be distributed as random numbers since they represent the deviations of the data from a model that should describe *all* of the deterministic structure in the data. The residuals allow for better assessment of model fit because small systematic errors are not hidden by the larger scale of the plot that is obtained when the data are plotted. To detect different kinds of departures the model may make from the data, the residuals should be plotted against each of the predictor variables in the model, which is HRTEM CD in this case, as well as any other variables that have been recorded but have not been included in the model. Other residual plots that are also part of a thorough model validation include run-order, lag, and normal probability plots [11].

The residuals from the model illustrated in Fig. 8 plotted versus the predictor variable HRTEM CD are shown in Fig. 9 to illustrate the characteristics of the Mandel fit of SEM CD to HRTEM CD. The points associated with each of the four chips, on which the respective six-feature measurements were made, are distinguished by the styles in the legend. Although the *overall* distribution of the residuals appears to be fairly random in Fig. 9, in support of the linear model, it is clear that all of the residuals for chip G1 are positive, whereas all of the residuals for chip D1 are negative. This behavior indicates that the straight-line model represented by (1) is not a statistically acceptable fit to the data. Use of this model in the intended manner would generally not provide reliable estimates of the uncertainties of the HRTEM-CDs from new incoming SEM transfer metrology measurements.

However, the results that have been obtained are consistent with a model in which the six SEM CD measurements that are extracted from a single test structure have a fixed component that is dependent on the condition under which the imaging was performed. Whereas the images of all six features from each test structure were obtained under almost identical conditions, this is almost certainly not true for the SEM instruments under which each of the four different chips was imaged. Therefore, it can be anticipated that a second measurement cycle could be implemented with an experimental design that more adequately maintains the uniformity of the instrument conditions under which the measurements are made on the respective chips. The high correlation between the SEM and HRTEM results shown in Fig. 8 suggests a high probability of future success by the use of SEM as the transfer metrology.

The most likely cause of the observed chip-based grouping of the residuals that has been shown in Fig. 8 is the contamination of the feature from hydrocarbon deposition during SEM imaging [12], [13]. This phenomenon inflates the observed linewidths to an extent that is dependent, among other things, on the time the operator chooses to allow the scanning electron beam to dwell on the features of the test structure. The next section presents evidence that the pattern of changes in an SEM CD that have been observed here appears to have been produced by failing to maintain SEM-beam exposure times at the same level for all four test-structure chips.

C. Measurement of the Deposition Rate of Hydrocarbon Contamination

The rate of hydrocarbon deposition depends on the imaging condition of the SEM instrument that is being used, as well as on the condition of the specimen being observed. In particular, insulating features such as those used here tend to encourage the phenomenon of "charging," which often enhances the hydrocarbon deposition rate. Whatever the source or sources of the contamination are, its effect generally monotonically increases with the time for which a measured feature is exposed to the scanning electron beam.

Accordingly, a study was made of the apparent CD inflation induced on a selection of features of the type used for this calibration study by an SEM instrument similar, but not identical, to that which was used. The same beam acceleration voltage and related imaging parameters were employed throughout.

In the contamination-rate study, the features were those embedded in test structures similar to the ones shown in Fig. 1 but were located on a fifth chip. Specifically, features F1 through F3 in Fig. 3, and then features F4 through F6, were imaged in similar operating conditions of the SEM instrument.[1] However, in this hydrocarbon deposition study, similar pairs of images were captured from the same test structure in another 11 measurement cycles. A clear indication of CD inflation during the progression through the 12 measurement cycles is evident in Fig. 10, which indicates that the regular growth in CD is approximately 2 nm per cycle for all six features. Since the magnitude of the per-cycle CD inflation is approximately of the same order as the differences in the grouping of the residuals in Fig. 9, it is now considered quite probable that the latter could have been caused by failure to ask the operators to control the imaging process with regard to maintaining SEM-beam exposure times at the same level for all test structures that were used.

In retrospect, specifying this level of control would seem to be an obvious measure to take. However, the original intention of SEM imaging in the broader project was only to screen the various test structures for feature CD uniformity.

[1]Whereas, in principle, it would have been possible to image all six features in the same exposure, this would have required a magnification of approximately 7500. Reducing the field size so that there were only three features in each image made it possible to increase magnification to 15 000. This increased level of magnification offered benefits that more than outweighed the logistics of imaging the target twice in each cycle.

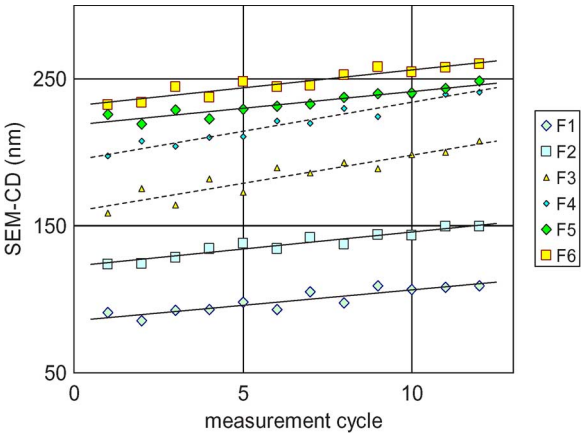

Fig. 10. Measured CD inflation during the progression through 12 measurement cycles indicates that the regular growth in CD is approximately 2 nm per cycle for all six features.

D. Caveat Calibrator

The purpose of the analyses reported here was to obtain an assessment of the CD uncertainties for the HRTEM/SEM traceability path and to compare this assessment with that provided by the established HRTEM/AFM alternative in the same application. Although closure on this issue has yet to be achieved, extremely promising results and valuable understanding that will contribute to a more definitive experiment were obtained. A broader exposition of *Recommendations to the User* in this regard has been issued by the authors elsewhere [14].

VI. Summary

CD measurements were made with both HRTEM and SEM imaging tools on sets of test-structure features that were replicated in monocrystalline silicon and had linewidths between 40 and 240 nm. The former provide absolute measurements traceable to the SI meter, whereas the latter serve for transfer metrology. Although advanced AFM metrology has proven to be a superior transfer metrology tool for CD calibration purposes, traceability paths to HRTEM measurements using an alternative transfer metrology such as SEM are technically interesting and worthy of assessment for certain calibration applications having less demanding uncertainty requirements. An important figure of merit for any traceability path is the uncertainty that is attributed to the CD value that has been calibrated. Ideally, all other things being equal, this value should be as small as possible. Industry's needs are application dependent; however, the most exacting current requirements are 1 nm. This matches the capability of the single-crystal CD reference material (SCCDRM) approach when AFM is used as the transfer metrology.

The new test structure reported here was designed to facilitate CD extraction from six features, having drawn linewidths staggered by 30 nm, from a single HRTEM image. The test chip pattern is replicated in the device layer of a (110) SIMOX-based test chip vehicle. The design of the test structure facilitates measurements of the CDs of all six features from a single HRTEM-imaging membrane preparation, which offers significant cost savings. Complete HRTEM CD measurement cycles were performed on four of the new test structures. In addition to the change in the HRTEM-imaging procedure, the lattice counting procedure was changed to ensure that no avoidable uncertainties were introduced to the final CD values from the HRTEM CD extraction procedure. The agreement in the extracted CDs from multiple counters was below 1 nm for the structures, which is a significant portion of the reduction in overall uncertainties in the CDs.

However, in this paper, the SEM CDs were extracted from the images of a selection of 24 features on four test structures on four different chips and were captured by different operators at different times. The SEM CDs that were extracted from the images were compared with the CDs that were determined from HRTEM imaging. Analysis of residual plots from linear least squares regression of SEM CD versus HRTEM CD indicates that the linear model did not adequately represent the data points because of the chip-based grouping of the residuals shown in Fig. 9. This outcome prevents a definitive evaluation of the uncertainties that are attributable to the practice of using SEM imaging as a transfer metrology. We conclude that variable hydrocarbon deposition rates probably have the leading responsibility for this result partly because the SEM operators were not given explicit instructions on maintaining identical image-capture conditions, including exposure time, partly because there is no fundamental physical reason for the measurements to be inconsistent with a linear model and because this test chip implementation has been shown by us to be vulnerable to such deposition. The overall correlation between SEM and HRTEM is judged to be sufficiently promising that substantially reduced uncertainties could be achieved if measures to minimize or controllably maintain the SEM exposure conditions are implemented.

Acknowledgment

The authors would like to thank the editorial reviews provided by National Institute of Standards and Technology (NIST) staffers D. Blackburn, R. Thurber, and E. Secula. They would also like to thank D. Leber of NIST and B. Bunday of Semiconductor Manufacturing Technology (SEMATECH) for technical reviews. J. Villarrubia and A. Vladar of NIST provided valued technical recommendations. M. Bennett and J. Allgair of SEMATECH are acknowledged for their support and encouragement. Extensive assistance-in-kind was provided by VLSI Standards, Inc., and SEMATECH. B. Bunday of SEMATECH is also acknowledged for helpful comments on the rates of hydrocarbon deposition by SEM CD tools. The authors acknowledge the contributions made by W. M. Tan during her participation in the NIST Summer Undergraduate Research Fellowship program.

References

[1] P. J. Mohr and B. N. Taylor, "CODATA recommended values of the fundamental physical constants: 1998," *J. Phys. Chem. Ref. Data*, vol. 28, no. 6, pp. 1713–1852, Nov. 1999.

[2] P. J. Mohr and B. N. Taylor, "CODATA recommended values of the fundamental physical constants: 1998," *Rev. Mod. Phys.*, vol. 72, no. 2,

pp. 351–495, Apr. 2000. [Online]. Available: http://www.physics.nist.gov/constants

[3] R. G. Dixson, "CD-AFM reference metrology at NIST and SEMATECH," *Proc. SPIE*, vol. 5752, pp. 324–336, 2005.

[4] R. A. Allen, T. J. Headley, S. C. Everist, R. N. Ghoshtagore, M. W. Cresswell, and L. W. Linholm, "High-resolution transmission electron microscopy calibration of critical dimension (CD) reference materials," *IEEE Trans. Semicond. Manuf.*, vol. 14, no. 1, pp. 26–31, Feb. 2001.

[5] R. A. Allen, A. Hunt, C. E. Murabito, B. Park, W. F. Guthrie, and M. W. Cresswell, "Extraction of critical dimension reference feature CDs from new test structure using HRTEM imaging," in *Proc. IEEE Int. Conf. Microelectron. Test Struct.*, Leuven, Belgium, Apr. 2005, pp. 5–10.

[6] R. A. Allen, B. A. am Ende, M. W. Cresswell, C. E. Murabito, T. J. Headley, W. F. Guthrie, L. W. Linholm, C. E. Hood, and E. H. Bogardus, "Test structures for referencing electrical linewidth measurements to silicon lattice parameters using HRTEM," *IEEE Trans. Semicond. Manuf.*, vol. 16, no. 2, pp. 239–248, May 2003.

[7] J. Mandel, *The Statistical Analysis of Experimental Data*. New York: Dover, 1964, pp. 288–292.

[8] J. Mandel, "Fitting straight lines when both variables are subject to error," *J. Qual. Technol.*, vol. 16, no. 1, pp. 1–13, Jan. 1984.

[9] J. Mandel, *Evaluation and Control of Measurements*. New York: Marcel Dekker, 1991, pp. 87–94.

[10] B. Bunday, W. G. Banke, C. Archie, G. Cao, C. Hartig, J. Villarrubia, A. Vladár, and B. Singh, *Unified Advanced Critical Dimension Scanning Electron Microscope (CD-SEM) Specification for Sub-90 nm Technology*. Austin, TX: Int. SEMATECH, 2004, pp. 19–26. Technology Transfer #04114595A-ENG.

[11] *NIST/SEMATECH e-Handbook of Statistical Methods*, Feb. 2005. [Online]. Available: http://www.itl.nist.gov/div898/handbook/

[12] M. Tortonese, Y. Guan, and J. Prochazka, "NIST-traceable calibration of CD-SEM magnification using a 100-nm pitch standard," in *Proc. SPIE—Metrology, Inspection, Process Control Microlithography XVII*, D. J. Herr, Ed., May 2003, vol. 5038, pp. 711–718.

[13] A. E. Vladar, M. T. Postek, and R. Vane, "Active monitoring and control of electron-beam-induced contamination," in *Proc. SPIE—Metrology, Inspection, Process Control Microlithography XV*, N. T. Sullivan, Ed., Aug. 2001, vol. 4344, pp. 835–843.

[14] M. W. Cresswell, W. F. Guthrie, R. G. Dixson, R. A. Allen, C. E. Murabito, B. Park, and J. V. Martinez De Pinillos, *Report of Investigation of RM 8111: Single-Crystal Critical Dimension Prototype Reference Materials*. Gaithersburg, MD: Nat. Inst. Stand. Technol., Mar. 2, 2005.

Michael W. Cresswell (M'66–SM'96–F'01–LF'03) received the Ph.D. degree in physics from the Pennsylvania State University, University Park, in 1965 and the MBA degree from the University of Pittsburgh, Pittsburgh, PA, in 1977.

He is a Physicist with the IC Technology Group at the National Institute of Standards and Technology (NIST), Gaithersburg, MD. He spent 19 years working in bipolar power devices, flat-panel displays, and IC process development. At NIST, he is developing reference materials for nanometer-level metrology for submicrometer feature placement, linewidth, and overlay. He is the holder of 25 patents in the field of semiconductor-fabrication technology.

Dr. Cresswell is a member of the American Physical Society.

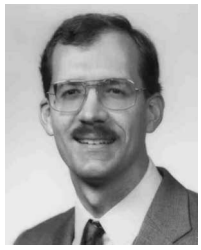

Richard A. Allen (M'85–SM'02) received the B.S. and M.S. degrees in physics from Rensselaer Polytechnic Institute, Troy, NY, in 1982 and 1984, respectively.

He was with Jet Propulsion Laboratory, Pasadena, CA, where he developed test structures for *in situ* monitoring space radiation effects in the Very Large Scale Integration Technology Group, as well as with College Park Software, Altadena, CA, where he worked on the development of list processing-based expert systems tools. Since June 1990, he has been with Semiconductor Electronics Division, National Institute of Standards and Technology, Gaithersburg, MD. His present interests include developing metrology test structures for microfluidics, MEMS, and microelectronics applications.

Mr. Allen is a member of the American Physical Society.

William F. Guthrie received the B.A. degree in mathematics from Case Western Reserve University, Cleveland, OH, in 1987 and the M.S. degree in statistics from The Ohio State University, Columbus, in 1990.

He is a Statistician with the Statistical Engineering Division, National Institute of Standards and Technology (NIST), Gaithersburg, MD. For the past 17 years, he has collaborated with NIST scientists and engineers on applied research in a wide range of areas, including semiconductor and microelectronics applications, building materials applications, and chemical science applications. His statistical interests include uncertainty assessment, Bayesian statistics, design of experiments, calibration, modern regression methods, and statistical computation.

Christine E. Murabito is currently working toward the B.S. degree in computer science from the University of Maryland University College, College Park.

She is an Applications Developer with the Semiconductor Electronics Division, National Institute of Standards and Technology (NIST), Gaithersburg, MD. At NIST, she writes data analysis programs to extract the electrical linewidth of silicon test structures, as well as assisting with other research. She also develops databases that store measurement data, SEM images, and processing information of silicon test structures and can be queried to find the optimal processing procedure for producing CDs with low uncertainty.

Ronald G. Dixson received the Ph.D. degree from Yale University, New Haven, CT, in 1994.

For the last 13 years, he has been a Staff Scientist with the Precision Engineering Division, Manufacturing Engineering Laboratory, National Institute of Standards and Technology (NIST), Gaithersburg, MD, primarily working on atomic force microscope (AFM) dimensional metrology and standards development, including the NIST Calibrated Atomic Force Microscope Project. Between 2001 and 2004, he was the first NIST Guest Scientist with SEMATECH, where he developed a CD-AFM-based reference measurement system and utilized this system for the 2004 release of single crystal critical dimension reference materials to SEMATECH member companies. His research interests are calibration methods, traceability, and uncertainty analysis in AFM dimensional metrology.

Dr. Dixson is a member of the American Physical Society and the International Society for Optical Engineering.

Amy Hunt, photograph and biography not available at the time of publication.